Dynamic myosin activation promotes collective morphology and migration by locally balancing oppositional forces from surrounding tissue

George Aranjuez[a,b,†], Ashley Burtscher[a], Ketki Sawant[c], Pralay Majumder[a,‡,*], and Jocelyn A. McDonald[a,b,c,*]

[a]Department of Cellular and Molecular Medicine, Lerner Research Institute, Cleveland Clinic, Cleveland, OH 44195; [b]Department of Genetics and Genome Sciences, School of Medicine, Case Western Reserve University, Cleveland, OH 44106; [c]Division of Biology, Kansas State University, Manhattan, KS 66506

ABSTRACT Migrating cells need to overcome physical constraints from the local microenvironment to navigate their way through tissues. Cells that move collectively have the additional challenge of negotiating complex environments in vivo while maintaining cohesion of the group as a whole. The mechanisms by which collectives maintain a migratory morphology while resisting physical constraints from the surrounding tissue are poorly understood. *Drosophila* border cells represent a genetic model of collective migration within a cell-dense tissue. Border cells move as a cohesive group of 6–10 cells, traversing a network of large germ line–derived nurse cells within the ovary. Here we show that the border cell cluster is compact and round throughout their entire migration, a shape that is maintained despite the mechanical pressure imposed by the surrounding nurse cells. Nonmuscle myosin II (Myo-II) activity at the cluster periphery becomes elevated in response to increased constriction by nurse cells. Furthermore, the distinctive border cell collective morphology requires highly dynamic and localized enrichment of Myo-II. Thus, activated Myo-II promotes cortical tension at the outer edge of the migrating border cell cluster to resist compressive forces from nurse cells. We propose that dynamic actomyosin tension at the periphery of collectives facilitates their movement through restrictive tissues.

INTRODUCTION

Cells frequently move in interconnected groups, termed collectives, to form and shape organs during development, remodel vessels during angiogenesis, and heal wounds (Friedl and Gilmour, 2009). Many types of cancer cells also invade as collectives, greatly contributing to tumor progression (Friedl *et al.*, 1995, 2012; Alexander *et al.*, 2013; Bronsert *et al.*, 2014; Clark and Vignjevic, 2015). The ability of cells to migrate in vivo, as single cells or as collectives, is influenced by the architecture of the three-dimensional tissue, whether it is loose or dense extracellular matrix (ECM) or even other cells (Friedl and Wolf, 2010; Wolf and Friedl, 2011; Wolf *et al.*, 2013; Clark and Vignjevic, 2015). Cells moving within tissues dynamically respond to physical changes in the local environment through deformability and adaptability of the cell itself (Friedl and Wolf, 2010; Doyle *et al.*, 2013; Wolf *et al.*, 2013). Cells in collectives often arrange into specific overall shapes, such as clusters, strands, or sheets, which need to be maintained for optimal movement of the

entire group (Friedl and Gilmour, 2009; Vedula *et al.*, 2012; Choi *et al.*, 2013; Leong *et al.*, 2013). Unlike individually migrating cells, cells in a collective must also stay together to coordinate their response to the microenvironment as a single unit. Because it is technically difficult to recreate the composition of tissues in vitro, the mechanisms that influence the maintenance of collective shape and organization in vivo and their effect on motility are still poorly understood.

Drosophila border cells are a relatively simple and genetically tractable model in which to address how collectives withstand the impact of surrounding tissue, stay together, and migrate within a native microenvironment. Border cells undergo a guided collective migration during late oogenesis (Montell *et al.*, 2012). The major subunit of the ovary is the egg chamber, which consists of a somatic, monolayer, follicular epithelium surrounding the germ line–derived nurse cells and the large oocyte at the posterior (Spradling, 1993) (Figure 1A). The polar cells, a specialized pair of follicle cells located at the anterior end of the egg chamber, secrete a cytokine signal to activate JAK/STAT signaling in adjacent follicle cells (Silver and Montell, 2001; Beccari *et al.*, 2002; Ghiglione *et al.*, 2002). The four to eight follicle cells with highest levels of JAK/STAT activation surround the polar cells and become migratory border cells. The border cell cluster then detaches from the epithelium and navigates between the 15 large nurse cells to eventually reach the oocyte (Figure 1A). Importantly, border cells stay together as a group during their entire migration. The cell polarity proteins Par-3 and Par-6, along with Jun kinase (JNK) signaling, promote cohesion of border cells and prevent individual cells from pulling away from the main group (Pinheiro and Montell, 2004; Llense and Martín-Blanco, 2008; Melani *et al.*, 2008). E-cadherin–based adhesion between border cells is critical to mechanically couple cells within the cluster (Cai *et al.*, 2014). Such adhesion induces front-to-back tension within the border cell cluster, allowing the group to respond to guidance cues and migrate directionally to the oocyte. E-cadherin also organizes the cluster by promoting adhesion of individual border cells to the centrally located polar cells.

Border cells remain as a cohesive cluster despite moving within the dense cellular environment of the egg chamber. To move forward, the border cell cluster needs to navigate between the closely packed nurse cells. The nurse cells serve as the migratory substrate for the border cell cluster, with differential and dynamic E-cadherin adhesion between the outer cluster membranes and nurse cell membranes providing optimal traction for border cells to move forward (Niewiadomska *et al.*, 1999; Cai *et al.*, 2014). The arrangement of nurse cells does not appear to allow much space for migration and further suggests that nurse cells apply force onto border cells. Despite this seeming limitation, the border cell cluster moves without difficulty while maintaining cohesion of the group. How the structural organization of the border cell group is preserved, and the extent to which this facilitates its movement through the confined setting of the egg chamber, is unclear.

Cells can withstand external mechanical pressure through the functions of internal force-generating proteins (Mohan *et al.*, 2015) such as nonmuscle myosin II (Myo-II). Myo-II is a hexameric protein complex that consists of three subunits: two heavy chains, two essential light chains, and two myosin regulatory light chains (MRLC; *Drosophila* Spaghetti Squash [Sqh]). The RhoA small GTPase activates Myo-II through kinases such as Rho-associated kinase (Rok; Amano *et al.*, 2010). Phosphorylation of MRLC/Sqh leads to maximal Myo-II activation (Vicente-Manzanares *et al.*, 2009). The active Myo-II motor establishes cortical tension of cells through its interaction with membrane-associated F-actin. For example, during mito-

sis, actomyosin tension promotes the rounding of cells (Stewart *et al.*, 2011; Ramanathan *et al.*, 2015). Myo-II is also essential for migrating cells, polarizing the cell and promoting retraction of the trailing edge (Vicente-Manzanares *et al.*, 2009). The role for Myo-II in migrating collectives, however, appears to be more complex. RhoA-activated Myo-II helps organize mechanical tension at the group level to prevent nonleading cells from forming migratory protrusions (Omelchenko *et al.*, 2003; Friedl *et al.*, 2014; Reffay *et al.*, 2014). Elevated Myo-II at cell contacts between A431 cancer cells inhibits their ability to invade collectively, thus promoting single-cell migration (Hidalgo-Carcedo *et al.*, 2011). Most of these studies were performed with cells in culture, either on two-dimensional surfaces or in simplified three-dimensional matrices. At present, the degree to which these findings apply to collectives moving through complex endogenous tissues and whether Myo-II-dependent cortical tension has additional roles, if any, are still open questions.

We report here that live border cells maintain a specific overall structure throughout their entire migration that requires highly dynamic Myo-II activity. The surrounding nurse cells produce forces that impinge on the border cell cluster. In response, border cells up-regulate activated Myo-II at the cluster periphery. The spherical border cell cluster shape can be perturbed by various genetic manipulations of Myo-II function, either in the nurse cells or in border cells themselves. Such altered cluster morphology correlates with reduced ability of some border cells to migrate. Dynamic phosphorylation of Sqh/MRLC through Rok is required for cluster morphology. Moreover, periodic waves of Myo-II enrichment occur at the outer edges of the cluster coincident with membrane contraction. We propose that cycles of dynamic actomyosin activation and inactivation at the cluster periphery provide optimal levels of cortical tension at the level of the collective. This allows border cells to achieve a specific compact morphology that enables the cluster to withstand forces from the surrounding tissue and may help the cluster to efficiently migrate.

RESULTS

Nurse cells mechanically influence border cell cluster migration

The egg chamber is a cell-dense tissue, raising the question of whether the nurse cell environment mechanically influences the border cell cluster during its migration. We first addressed how nurse cells are organized with respect to border cells during the stages that border cells migrate. We stained live egg chambers with FM 4-64 dye, which labels many, though not all, cell membranes. Three-dimensional reconstruction of z-stack images shows that adjacent nurse cells are in tight contact with one another, with very little apparent space between the cells (Figure 1B and Supplemental Movie S1). The border cell cluster is located directly adjacent to, and is surrounded by, nurse cell membranes (Figure 1B). Live time-lapse imaging using differential interference contrast (DIC) optics to visualize the shapes of unstained cells reveals that border cells move efficiently between the 15 packed nurse cells (Figure 1A and Supplemental Movie S2; Montell *et al.*, 2012). Moreover, the nurse cells visibly deform when border cells pass between them (Supplemental Movie S2; Stonko *et al.*, 2015).

Given the tight association between border cells and the much larger nurse cells (Figure 1C), we asked whether nurse cells are able to mechanically influence border cells. The nurse cells are normally constrained by the surrounding squamous follicle cell epithelium; by the basement membrane located on the outside of the tissue, which serves as a so-called "molecular corset" for egg chamber growth; and by a muscle sheath that surrounds each string of egg chambers
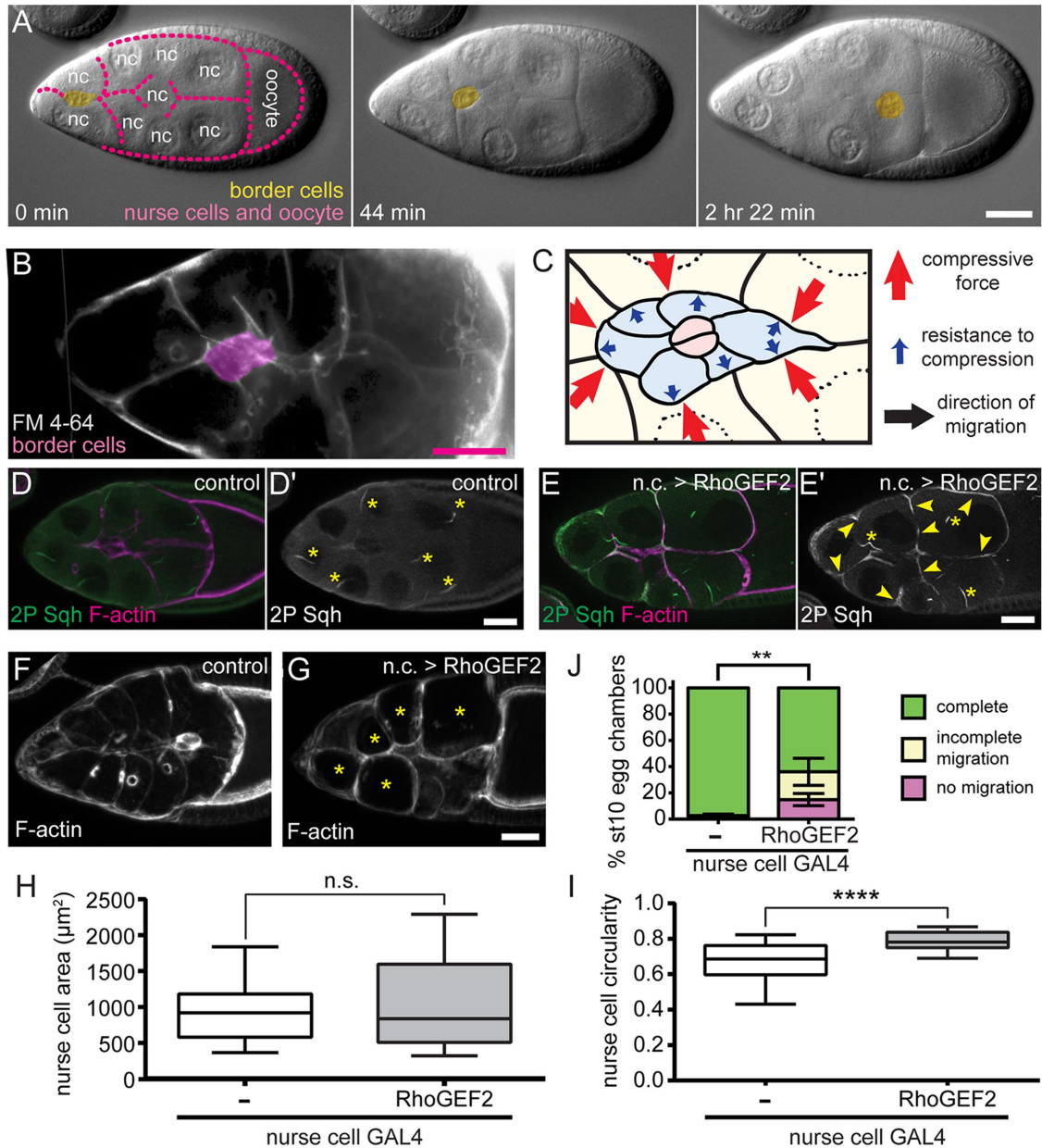
FIGURE 1: Nurse cells influence border cell cluster migration. (A) Frames from a DIC movie (Supplemental Movie S2) showing border cells (false-colored yellow) migrating between the nurse cells (nc; pink outlines) to reach the oocyte (*n* = 5 movies). The follicle cell epithelium surrounds the germ line. Scale bar: 40 µm. (B) Merged three-dimensional z-stack image of a live stage 9 egg chamber stained with the lipophilic FM 4-64 dye; the dye labels many, though not all, cell membranes. This image is taken from Supplemental Movie S1. Border cells, distinguished by enriched FM 4-64 staining (false-colored magenta), are closely surrounded by neighboring nurse cell membranes. The oocyte is to the far right. Scale bar: 20 µm. (C) Model of tissue-level forces between the border cell cluster (blue arrows) and the nurse cells (red arrows). Border cells are proposed to resist compression from nurse cells. Border cells are blue; central polar cells are pink; nurse cells are yellow; dashed lines indicate nurse cell nuclei. The direction of migration is to the right (black arrow). (D–E') 2P-Sqh expression in nurse cells. Stage 9 egg chambers stained for 2P-Sqh (green in D and E) and phalloidin to label F-actin (magenta in D and E). (D and D') Control egg chambers have low levels of 2P-Sqh at nurse cell membranes. (E and E') Elevated 2P-Sqh staining (arrowheads) at cortical nurse cell membranes in a nurse cell (n.c.) > RhoGEF2 egg chamber (*n* = 24). Filamentous 2P-Sqh within nurse cell cytoplasm (asterisks in D' and E') is likely nonspecific staining. Scale bars: 20 µm. (F and G) RhoGEF2 expression in nurse cells causes the cells to become rounder than normal (asterisks). Late stage 9 control (F; nurse cell GAL4/+) and stage 10 RhoGEF2 (G; nurse cell GAL4/ UASp-RhoGEF2) egg chambers stained with phalloidin to label F-actin. Scale bar: 20 µm. (H and I) Measurements of nurse cells, represented as box-and-whisker plots. The whiskers represent the minimum and maximum, the box extends from the 25th to the 75th percentiles, and the line indicates the median measurement. Nurse cells from control egg chambers (*n* = 29) and nurse cells from nurse cell > RhoGEF2 egg chambers (*n* = 26) were analyzed; not significant (n.s.), $p \geq 0.05$; ****, $p < 0.0001$; unpaired *t* test. (H) Quantification of the area of nurse cells in control and nurse cell > RhoGEF2 egg chambers. (I) Quantification of the circularity of nurse cells from control and nurse cell > RhoGEF2 egg
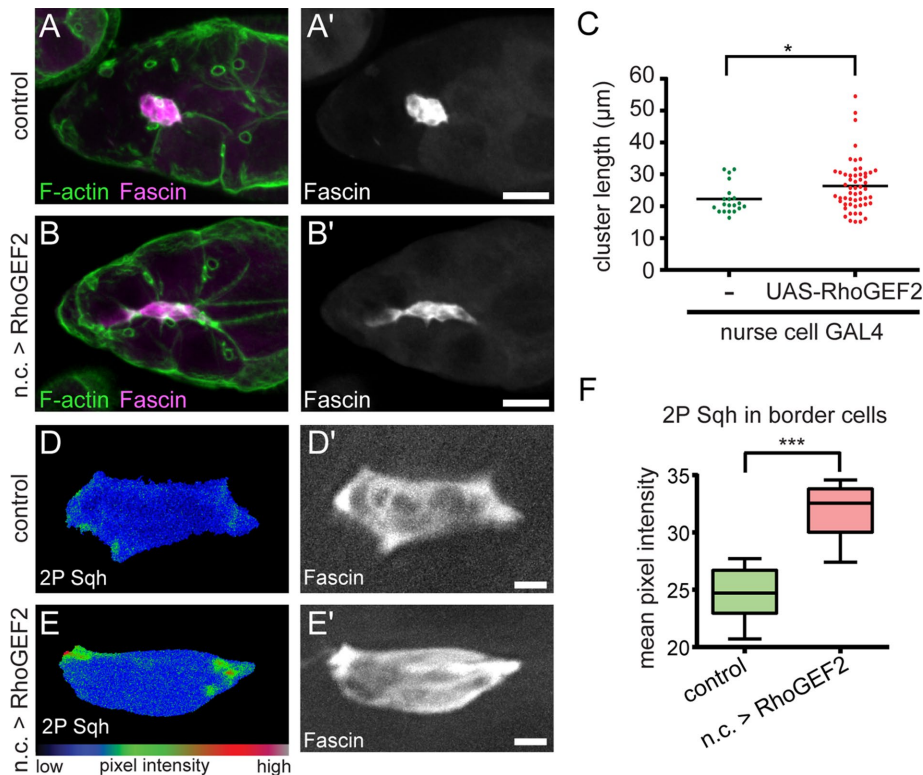
FIGURE 2: Border cells change shape and increase levels of activated Myo-II in response to nurse cells. (A–C) Elongation of wild-type border cell clusters upon increased contraction of nurse cells. Stage 9 control (nurse cell GAL4/+) and RhoGEF2 (nurse cell GAL4/UASp-RhoGEF2) egg chambers stained with phalloidin to label F-actin (green in A and B) and Fascin to mark border cells (magenta in A and B; white in A' and B'). Scale bars: 20 µm. (A and A') Control border cell cluster shape is normal. (B and B') Example of a border cell cluster that is elongated in a nurse cell > RhoGEF2 egg chamber. (C) Quantification of individual border cell cluster lengths from control ($n = 20$) and nurse cell > RhoGEF2 ($n = 55$) egg chambers. The line indicates the mean. *, $p < 0.05$; unpaired t test. (D–F) Elevated 2P-Sqh levels in border cells when the surrounding nurse cells express RhoGEF2. (D and E) The heat map shows the levels of low to high signal intensity of 2P-Sqh. (D' and E') The border cell cluster is defined by Fascin signal, which is expressed at low levels in nurse cells at this stage of egg chamber development (Cant et al., 1994). Scale bars: 5 µm. (F) Quantification of the mean 2P-Sqh pixel intensity within the border cell cluster (defined by Fascin staining) from control ($n = 8$) and nurse cell > RhoGEF2 ($n = 11$) egg chambers, represented as a box-and-whisker plot. The whiskers represent the minimum and maximum pixel intensity; the box extends from the 25th to the 75th percentiles; the line indicates the median measurement. ***, $p < 0.001$; unpaired t test.

with intracellular pressure, actomyosin-dependent contraction contributes to cell rounding and cortical tension (Stewart et al., 2011; Clark et al., 2014; Ramanathan et al., 2015). We therefore expressed RhoGEF2 in all nurse cells to ectopically increase the cellular contraction and tension of these cells. We used an antibody to phosphorylated Sqh (2P-Sqh) to confirm that this manipulation increases the levels of activated Myo-II in nurse cells compared with control (Figure 1, D, D', E, and E'). RhoGEF2 expression altered the shape but not the overall size of nurse cells, causing the cells to appear rounder than control (Figure 1, F and G, and Supplemental Movie S3). To analyze this directly, we measured the area (Figure 1H) and circularity (Figure 1I) of nurse cells. The area of the RhoGEF2-expressing nurse cells is unchanged, but these cells are significantly more circular than control nurse cells (median control = 0.68 vs. median nurse cell > RhoGEF2 = 0.78). Notably, we did not observe any visible gaps between RhoGEF2-expressing nurse cells, nor did the ring canals that connect nurse cells appear grossly abnormal (Supplemental Movie S3).

Elevating nurse cell contraction by RhoGEF2 expression impairs the ability of genetically wild-type border cells to complete their migration (Figure 1J). Whereas all border cells in control egg chambers reach the oocyte by stage 10 of oogenesis, ~40% of border cells in nurse cell > RhoGEF2 egg chambers either do not initiate migration or fail to reach the oocyte by stage 10. These data indicate that having optimal levels of nurse cell deformability is necessary for border cells to be able to migrate.

Border cells increase levels of activated Myo-II and undergo morphology changes in response to constraint by nurse cells

(Cetera and Horne-Badovinac, 2015; Andersen and Horne-Badovinac, 2016). Increasing the cellular contraction of nurse cells to increase nurse cell rigidity is expected to increase compressive forces along the migration path (Figure 1C). RhoGEF2 is a known activator of the *Drosophila* RhoA GTPase, which in turn activates Rok and Myo-II to drive cell shape changes (Hacker and Perrimon, 1998; Rogers et al., 2004). Myo-II activity upon cortical F-actin is known to promote force generation that is transmitted along actin cables to cell membrane anchors (Munjal and Lecuit, 2014). When coupled

Live migrating border cell clusters have a distinctly round shape that is maintained, with only minor deviations, for the entirety of their migration (Figure 1A and Supplemental Movie S2). This observation suggests that border cells require a specific morphology during their migration. Therefore we next asked what happens to the cluster in the more rigid environment of RhoGEF2-expressing nurse cells (Figure 1G). Border cells in fixed control egg chambers exhibit typical cluster morphology and length (Figure 2, A, A', and C; see *Materials and Methods*). Strikingly, however, egg chambers with

chambers. A value of 1.0 is a perfect circle, whereas a number close to 0.0 is an extremely elongated shape. (J) Quantification of border cell migration in egg chambers expressing RhoGEF2 in nurse cells (nurse cell GAL4/UASp-RhoGEF2; $n = 162$ egg chambers) compared with control (nurse cell GAL4/+; $n = 217$), shown as the percentage of stage 10 egg chambers with complete, incomplete, or no migration to the oocyte. A diagram illustrating the migration distance is shown in Supplemental Figure S1C. At least three trials were performed per genotype; $n \geq 50$ egg chambers per trial. **, $p < 0.01$; unpaired t test. Error bars: SEM. In this and all subsequent figures, anterior is to the left and the direction of migration is to the right.

nurse cells that express high levels of RhoGEF2 have a significant number of genetically wild-type border cell clusters that visibly become stretched along the migration pathway (Figure 2, B, B′, and C). Increased nurse cell tension thus constricts the shape of the border cell cluster during its migration.

Given that Myo-II can function as a mechanosensor and that physical constriction of cells in vitro can recruit Myo-II to the cell cortex (Laevsky and Knecht, 2003; Ren et al., 2009; Luo et al., 2012; Elliott et al., 2015; Kim et al., 2015), we next analyzed what happens to Myo-II when border cells become constrained by nurse cells. Myo-II, as visualized using a green fluorescent protein (GFP)-tagged sqh transgene (Royou et al., 2002), is highly enriched at outer membrane surfaces of the border cell cluster throughout all stages of migration (Supplemental Figure S1; Edwards and Kiehart, 1996; Majumder et al., 2012). Drosophila Sqh is phosphorylated at either Ser-21 (1P) or at both Thr-20/Ser-21 (2P), which are equivalent to Thr-18/Ser-19 on mammalian MRLC (Jordan and Karess, 1997; Zhang and Ward, 2011). Phosphorylation at the 1P and/or 2P sites activates Myo-II. Therefore we examined activated Myo-II in wild-type border cells under conditions of elevated confinement. As described above, we increased nurse cell tension and contraction by expressing RhoGEF2 only in nurse cells. Next we analyzed border cells from nurse cell > RhoGEF2 egg chambers stained for 2P-Sqh. The border cell–specific marker, Fascin, allowed us to define and assess the levels of activated Myo-II only in border cells (Figure 2, D, D′, E, and E′).

When contraction of nurse cells is increased through expression of RhoGEF2, border cell clusters exhibit more 2P-Sqh staining compared with control (Figure 2, D and E). Moreover, the most intense 2P-Sqh staining is found close to the cluster periphery (Figure 2E). Quantification of the mean pixel intensity for 2P-Sqh confirms that the border cells in nurse cell > RhoGEF2 egg chambers have significantly elevated 2P-Sqh levels (Figure 2F). Thus, elevated pressure from the nurse cells increases the levels of activated Myo-II in border cells. These data support the idea that the nurse cells physically influence the morphology of the border cell cluster and that border cells respond through Myo-II activation. Together our results suggest a model in which the border cell cluster has a distinct morphology that is influenced by the nurse cell environment and that may be important for its movement within the tissue.

The border cell cluster requires Myo-II to maintain morphology during migration

We next asked how border cells attain their characteristic cluster shape. We hypothesized that the specific morphology of the border cell cluster contributes to the ability of border cells to resist forces from the surrounding tissue (Figure 3A). Myo-II is required for border cell migration and is highly expressed in the cluster (Figure 3B; Edwards and Kiehart, 1996; Fulga and Rørth, 2002; Majumder et al., 2012). Moreover, phosphorylated Myo-II is elevated in response to nurse cell–driven constriction (Figure 2, D–F). We thus reasoned that localized cortical actomyosin tension within the border cell group could serve as a mechanism to oppose compressive forces imposed on them by adjacent nurse cells (Figure 1C and Figure 3A).

To investigate the extent to which Myo-II contributes to the shape of the migrating border cell cluster, we knocked down Myo-II function using a GAL4-driven upstream activation sequence–RNA interference (UAS-RNAi) transgene that significantly reduces sqh RNA levels in vivo (Supplemental Figure S2, A and B). We also validated specific knockdown in border cells. Expression of sqh RNAi, driven by c306-GAL4 in border cells and anterior follicle cells (Supplemental Figure S3), shows reduced levels of phosphor-

ylated Sqh in border cells (Supplemental Figure S2C). In agreement with previous studies, sqh RNAi impairs the detachment of border cells from the follicle cell epithelium, border cell migration to the oocyte, and retraction of leading-edge protrusions (Supplemental Figure S4, A–E; Edwards and Kiehart, 1996; Fulga and Rørth, 2002; Majumder et al., 2012). A large proportion of sqh RNAi border cell clusters visibly elongate along the migration pathway compared with control (Figure 3, C and D). We then measured the length of border cell clusters along the migration axis from the front to back of the group, excluding visible cellular protrusions, in fixed egg chambers (see Materials and Methods). Control border cell clusters are compact and measure ~20–30 μm in length (Figure 3, C and E). In contrast, sqh-deficient clusters can reach lengths up to 80 μm, more than twice the control cluster length (Figure 3, D and E). We confirmed the requirement of sqh for proper cluster morphology by producing mosaic clones of a loss-of-function sqh allele (sqh^AX3). We find that 18% of border cell clusters containing at least two or three sqh^AX3 homozygous mutant cells are elongated, whereas control mosaic clusters are compact (Figure 3, F and G). Clusters that contain only mutant sqh^AX3 border cells are rarely found (Majumder et al., 2012), which may account for the lower frequency of elongated clusters compared with sqh RNAi. The stretched-out cluster shape produced by loss of Myo-II is distinct from mutants that disrupt adhesion between individual cells and cause the border cell cluster to partially or completely pull apart (Pinheiro and Montell, 2004; Llense and Martín-Blanco, 2008; Cai et al., 2014). Indeed, border cells deficient for sqh do not break away from the cluster (Figure 3, D and G), further indicating that Myo-II does not play a major role in keeping border cells adhered together in a group.

Next we performed live time-lapse imaging to address the role for Myo-II in maintaining the dynamic morphology of the cluster during migration (Figure 3, H and I; Supplemental Movies S4 and S5). Once migration begins, sqh RNAi border cell clusters noticeably become more elongated than control. We quantified the variability in cluster length during the entire movie, primarily focusing on border cell clusters that had detached or were in the process of detaching from the epithelium (Figure 3J). Control border cells consistently retain a compact shape, with minimal variation in the length of the cluster. In contrast, when sqh RNAi border cells migrate, cluster length is highly variable and can stretch up to 80 μm long, in agreement with measurements from fixed egg chambers (Figure 3, E and J). Together these data show that loss of Myo-II disrupts the compact morphology of border cell clusters during their migration.

Activated Myo-II is required for cell and cluster morphology of border cells

The results described above suggest that Myo-II promotes cluster shape and show that nurse cell constriction recruits activated Myo-II to the cluster periphery (Figure 2, D–F). Next we asked to what extent is specific regulation of Myo-II activity required for normal border cell cluster shape. The regulatory light chain component Sqh (MRLC) undergoes dynamic cycles of phosphorylation by kinases and dephosphorylation by myosin phosphatase to, respectively, activate and inactivate Myo-II (Vicente-Manzanares et al., 2009). Rok is one of a number of serine–threonine kinases that phosphorylate the 1P and 2P sites of Sqh/MRLC (Amano et al., 1996; Ueda et al., 2002). Because Rok is required for border cell migration (Supplemental Figure S4A; Majumder et al., 2012), we wanted to know whether Rok is the relevant kinase for Myo-II function in cluster morphology. Activated Myo-II (1P- and 2P-Sqh) localizes primarily in intense foci restricted to the cluster periphery, adjacent to contacts
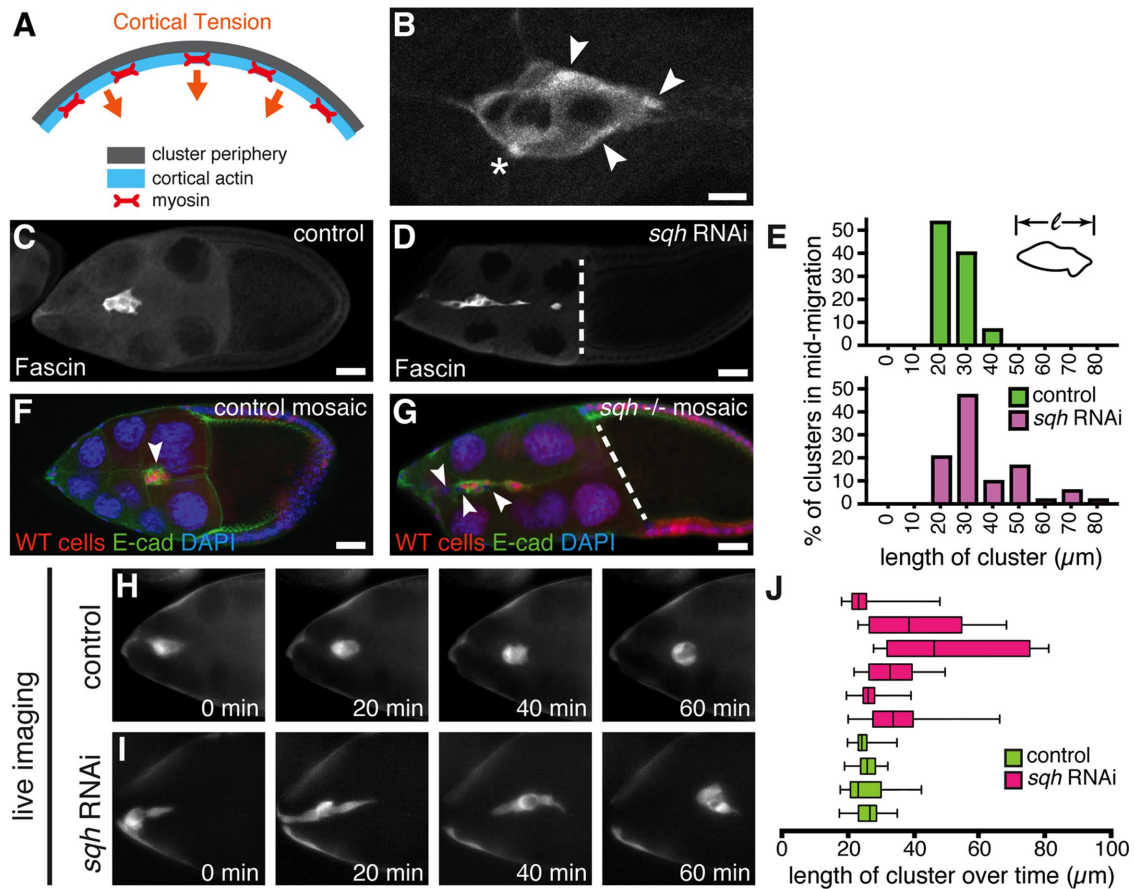
FIGURE 3: Myo-II maintains the migratory morphology of the border cell cluster. (A) Illustration of proposed mechanism by which Myo-II (red) and F-actin (blue) generate cortical tension to contract border cell cluster membranes (arrows). (B) Localization of Sqh:GFP in border cells during migration. Sqh:GFP is enriched in foci at the cluster periphery (arrowheads) and in polar cells (asterisk). Scale bar: 5 μm. (C–G) Knockdown or loss of *sqh* disrupts cluster shape. (C and D) Fascin labels border cells of stage 9 control (*c306*-GAL4, tsGAL80/+) and stage 10 *sqh* RNAi egg chambers (*c306*-GAL4, tsGAL80/+; UAS-*sqh* RNAi/+). (D and G) Dashed line indicates the anterior oocyte border. (E) Quantification of cluster length (*l*) along the axis of migration (schematic), shown as the percentage of control ($n = 30$) and *sqh* RNAi ($n = 75$) midmigration border cells in stage 9 egg chambers. (F and G) Examples of stage 9 *FRT 19A* control (F) and stage 10 *sqh^AX3* (G) mosaic mutant clusters ($n = 38$), costained for E-cadherin (E-cad; green) to label cell membranes and DAPI (blue) to show nuclei. Loss of nuclear RFP (red fluorescent protein; red) marks cell clones (arrowheads). Scale bars (C, D, F, and G): 20 μm. (H and I) Frames from control (H) and *sqh* RNAi (I) live movies (Supplemental Movies S4 and S5) showing migrating border cells (mCD8:GFP). (J) Quantification of the variability in cluster length from individual movies over time (~1 h duration), shown as box-and-whisker plots. The whiskers represent the minimum and maximum length within one movie; the box extends from the 25th to the 75th percentiles; the line indicates the median length measurement within that movie.

with the nurse cells (Figure 4, A–A″). We therefore examined Rok localization with respect to activated Myo-II. Using a functional Rok:GFP transgene (Bardet *et al.*, 2013), we find that Rok specifically localizes to the outer edge of the border cell cluster in a discontinuous pattern (Supplemental Figure S5, A″ and A‴). Rok:GFP coincides with some 1P and 2P Sqh foci (Supplemental Figure S5, A–A‴), consistent with the ability to activate Myo-II. In agreement with other migrating collectives (Hidalgo-Carcedo *et al.*, 2011; Reffay *et al.*, 2014), very little active Myo-II or Rok localizes at membrane contacts between border cells.

Given the specific localization of Rok to the cluster periphery, and colocalization with activated Myo-II, we next analyzed the requirement for Rok in the maintenance of border cell cluster morphology. Border cell clusters that express a kinase-dead version of Rok (Rok KD), or that contain mosaic mutant clones of a strong loss-of-function *Rok* allele (*Rok²*), result in elongated clusters (Figure

4, B and C). Thus the Myo-II–activating kinase Rok regulates border cell cluster shape during migration.

We next analyzed the degree to which the appropriate levels and/or localization of activated Myo-II contribute to cell and cluster shape of border cells. The small GTPase RhoA (*Drosophila* Rho1) activates Rok and thus influences Myo-II activation (Amano *et al.*, 1996; Ishizaki *et al.*, 1996; Matsui *et al.*, 1996). We therefore expressed a constitutively active form of RhoA (RhoA^V14) in border cells. Compared with control clusters, RhoA^V14 individual border cells are much rounder, and the overall cluster appearance is altered (Figure 4, D–G). Consistent with a previous report (Bastock and Strutt, 2007), 40% of RhoA^V14 border cells do not complete their migration (Supplemental Figure S4A). The overall levels of 1P- and 2P-Sqh are also elevated in RhoA^V14 border cell clusters compared with control (Figure 4, D–G and I). Moreover, activated Myo-II (1P- and 2P-Sqh) is mislocalized in RhoA^V14 clusters, with ectopic
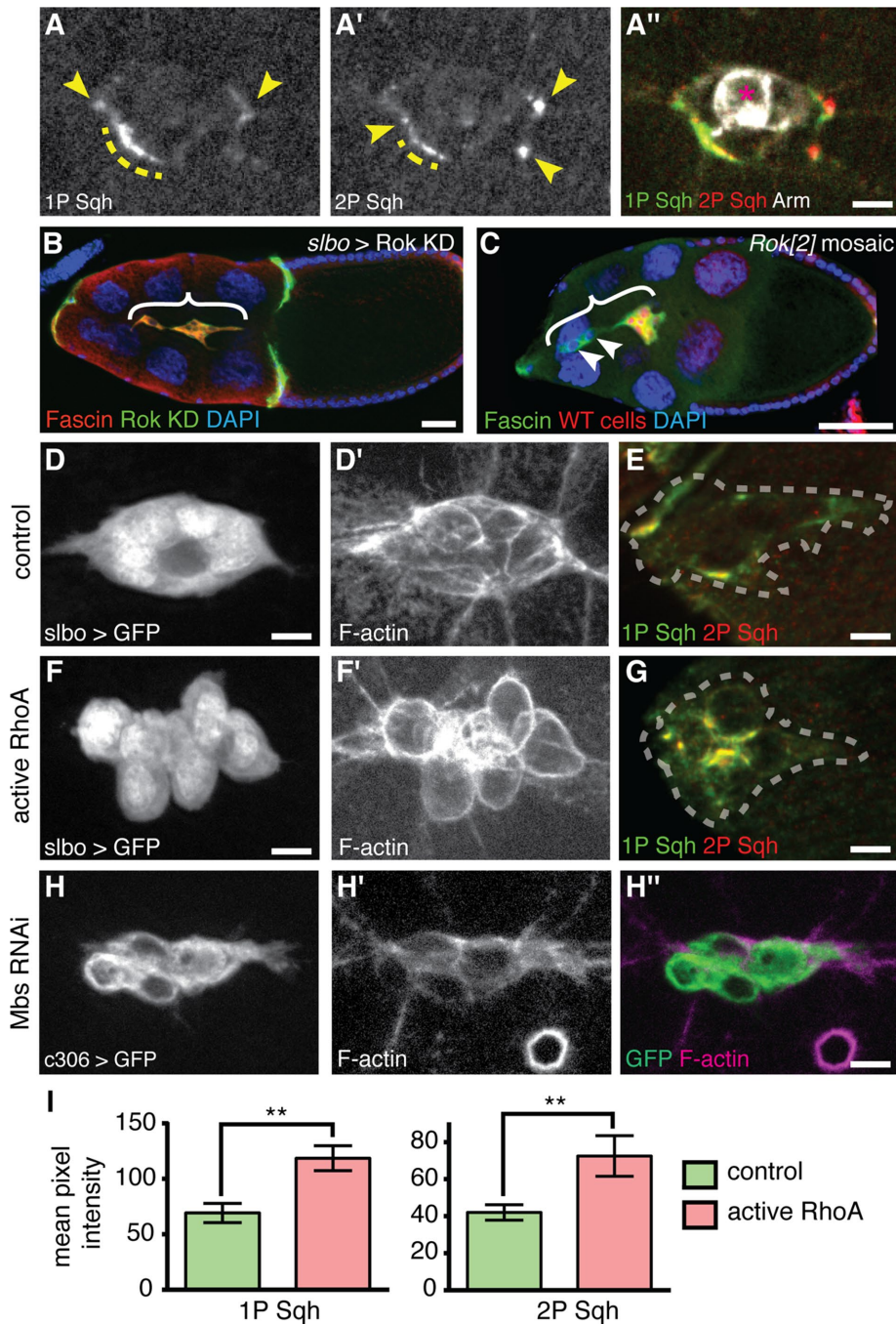
FIGURE 4: Cell and cluster morphology of border cells requires activated Myo-II. (A–A") Representative example of a stage 9 wild-type border cell cluster stained for 1P-Sqh (green) and 2P-Sqh (red). The 1P-Sqh and 2P-Sqh colocalize (yellow in A") and are enriched in discrete foci (arrowheads, dashed line) at the cluster periphery ($n = 17$). Armadillo (Arm; white in A") labels all cell membranes, including the central polar cells (asterisk). Scale bar: 5 μm. (B) Example of an elongated Rok KD cluster (bracket) in a *slbo*-GAL4/UAS-Venus:Rok KD stage 10 egg chamber. The border cells are stained for Fascin (red), Venus:Rok KD (green), and DAPI (blue nuclei). (C) Example of a cluster with stretched-out, trailing *Rok²* mutant border cells (loss of nuclear RFP; arrowheads) in a stage 9 egg chamber stained for Fascin (green) and DAPI (blue nuclei). Scale bars (B and C): 50 μm. (D–G) Activated RhoA causes rounded border cells and disrupts cluster shape. Stage 9 control (slbo-GAL4, UAS-mCD8:GFP/+) and active RhoA (slbo-GAL4, UAS-mCD8:GFP/UAS-Rho1^V14) border cells labeled by GFP (D and F) and F-actin (D' and F'). (E and G) The 1P- and 2P-Sqh localize to the periphery of control (E) but are mislocalized in constitutively active RhoA (G; $n = 19$) border cell clusters. Dashed lines indicate the cluster boundary. (H–H") Altered shape of *Mbs* RNAi (c306-GAL4/+; UAS-*Mbs* RNAi/UAS-mCD8:GFP) border cells ($n > 7$), marked by GFP (H; green in H") and F-actin (H'; magenta in H").

enrichment at membrane contacts between border cells (Figure 4, E and G). We confirmed that RhoA protein is misexpressed (Supplemental Figure S5, B–C'). Specifically, RhoA^V14 clusters have high levels of RhoA protein around each border cell, compared with a more general distribution in control clusters. Such altered localization supports the idea that RhoA^V14 activates Myo-II at individual border cell cortical membranes (Figure 4G). Border cells also have altered F-actin distribution (Figure 4F'), consistent with the known ability of mammalian RhoA both to promote F-actin assembly through the formin mDia (mammalian homologue of *Drosophila* Diaphanous) and Myo-II activity through Rok (Narumiya *et al.*, 2009).

To further address the importance of appropriate levels of activated Myo-II, we next inactivated myosin phosphatase. Myosin phosphatase consists of a catalytic protein phosphatase 1 subunit (PP1c) and a myosin-binding specificity subunit (Mbs) (Grassie *et al.*, 2011). Because myosin phosphatase dephosphorylates Sqh, loss of the phosphatase will result in increased levels of phosphorylated and activated Myo-II (Kimura *et al.*, 1996; Grassie *et al.*, 2011). Mbs is highly expressed in border cells, and RNAi knockdown elevates the levels of 1P-Sqh in the cluster (Majumder *et al.*, 2012). When we knocked down *Mbs* using RNAi, these clusters contained rounder border cells than normal (Figure 4, H–H"). Taken together, our results suggest that appropriate levels of activated Myo-II, as well as restriction of activity to the cluster periphery, promote the proper morphology of both individual border cells and the cluster as a whole.

Dynamically regulated Myo-II correlates with cluster shape and membrane deformation

Previous research on collectively migrating cells in vitro indicates that spatially localized Myo-II activation keeps collectives together as a functional unit and prevents their dissociation into single cells (Hidalgo-Carcedo *et al.*, 2011; Friedl *et al.*, 2014; Reffay *et al.*, 2014). In the case of collectives that migrate within tissues, such as border cells, it is unclear whether it is the levels/localization of active Myo-II or the dynamics of active Myo-II that are needed to maintain a migratory morphology. We therefore investigated the extent to which dynamic Myo-II activation

Scale bar (D–H"): 5 μm. (I) Mean pixel intensity of 1P- and 2P-Sqh measured in control ($n = 10$) and active RhoA ($n = 6$) border cell clusters. Error bars: SEM. **, $p < 0.01$; unpaired t test.
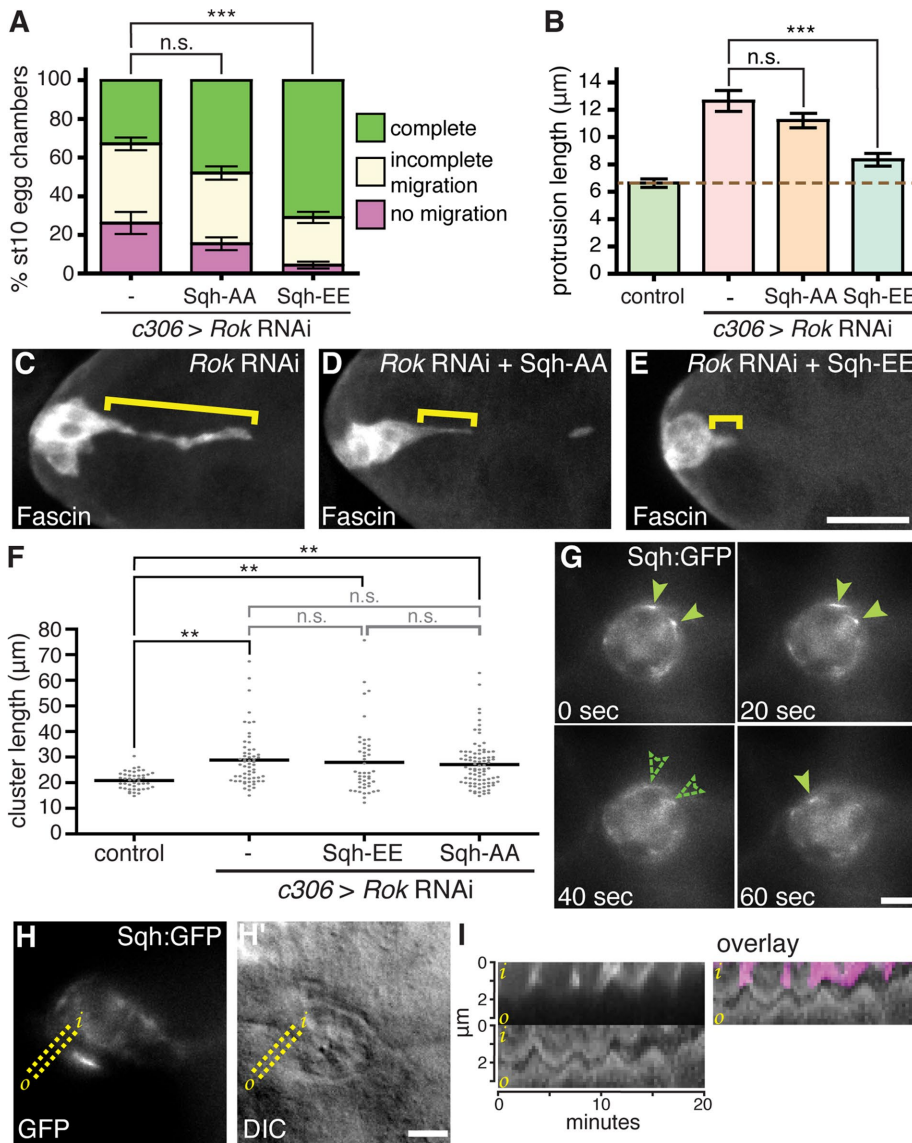
FIGURE 5: Requirement for dynamic cycles of activated Myo-II in cluster shape and membrane deflection. (A) Sqh-EE strongly suppresses the *Rok* RNAi migration defects. Quantification of complete, incomplete, and no migration in stage 10 *Rok* RNAi (*c306*-Gal4/+; UAS-*Rok* RNAi/+) egg chambers, with or without the indicated Sqh mutant transgenes. $n \geq 50$ egg chambers in each of three trials; not significant (n.s.), $p \geq 0.05$; ***, $p < 0.001$; one-way ANOVA with Dunnett test compared with "complete migration." (B–E) Sqh-EE rescues the *Rok* RNAi border cell protrusion-length defects. (B) Quantification of mean protrusion length in the indicated genotypes. Dashed line shows the mean protrusion length of control (*c306*-GAL4/+). $n \geq 86$ protrusions per genotype; n.s., $p \geq 0.05$; ***, $p < 0.001$; one-way ANOVA with Dunnett test. Error bars in A and B: SEM. (C–E) Stage 9 *Rok* RNAi egg chambers, with or without the indicated Sqh mutant transgenes, stained for Fascin to label border cells and protrusions (brackets). Scale bar: 20 μm. (F) Sqh-EE and Sqh-AA did not alter the *Rok* RNAi cluster elongation defect. Quantification of individual border cell cluster length measurements in the indicated genotypes. The line indicates the mean. $n \geq 46$ clusters per genotype; n.s., $p \geq 0.05$; **, $p < 0.01$; one-way ANOVA with Dunnett test. (G) Consecutive frames from a Sqh:GFP movie at the indicated times. Two foci of Sqh:GFP (arrowheads) were tracked at the cluster periphery until they disappeared (arrowhead outlines). A new foci appears in the last frame. (H and H') Frame from a time-lapse Sqh:GFP movie (Supplemental Movie S6) simultaneously imaged by fluorescence microscopy (H) and DIC (H') optics to visualize cell membranes ($n = 6$). Scale bars (G and H): 5 μm. The boxed region corresponds to the kymograph shown in I, with the outside ("o") and inside ("i") labeled to provide orientation. (I) Kymograph of the GFP (top) and DIC (bottom) channels from the boxed region in H and H' over time (minutes). Sqh:GFP (magenta, overlay) correlates with deflection of the cluster membrane ($n = 9$ egg chambers). Orientation as in H and H'.

contributes to border cell cluster morphology during migration. We used phosphorylation-mutant variants that lock Sqh/MRLC into either unphosphorylated (Sqh-AA) or constitutively phosphorylated (Sqh-EE) forms and that are driven by the endogenous *sqh* promoter (Jordan and Karess, 1997; Winter *et al.*, 2001). Because we wanted to manipulate the levels of activated Myo-II, rather than Myo-II protein itself, we knocked down the Myo-II activator *Rok* in border cells. Expression of *Rok* RNAi strongly depletes *Rok* mRNA in vivo (Supplemental Figure S2, D and E) and reduces 1P-Sqh levels in border cells (Majumder *et al.*, 2012). *Rok* RNAi disrupts border cell migration (Figure 5A and Supplemental Figure S4A; Majumder *et al.*, 2012) and produces long protrusions that fail to retract (Figure 5, B and C). Moreover, similar to our observations with *Rok* mutants (Figure 4, B and C), *Rok* RNAi border cell clusters are more elongated compared with control (Figure 5F).

We next asked whether the phosphomimetic or nonphosphorylatable mutant forms of Sqh could rescue the *Rok*-dependent phenotypes. Introduction of one copy of Sqh-EE strongly, though not completely, suppresses *Rok* RNAi migration (Figure 5A) and protrusion defects (Figure 5, B, C, and E), consistent with the known role for Rok in phosphorylating Sqh (Amano *et al.*, 1996; Winter *et al.*, 2001). As expected, Sqh-AA has little effect (Figure 5, A, B, and D). Surprisingly, neither Sqh-EE nor Sqh-AA is able to alter the length of *Rok* RNAi clusters (Figure 5F). Importantly, Sqh-EE, visualized by a FLAG tag, localizes to the cluster periphery (Supplemental Figure S5, D–D'''). The distribution of Sqh-EE is similar to that observed for endogenous 2P-phosphorylated Sqh (compare with Figure 4, A–A'''), indicating that the inability to rescue the *Rok* RNAi cluster shape defects is not due to mislocalization of the Sqh-EE transgene. These data together demonstrate that Rok promotes cluster shape through activation of Myo-II.

Our finding that phosphomimetic Sqh cannot rescue the *Rok* RNAi–dependent elongated cluster phenotype suggests that cycling between phosphorylated active and dephosphorylated inactive forms of Myo-II maintains the shape of the border cell cluster. To further test the idea that dynamic regulation of Myo-II activity is required for cluster morphology, we next analyzed the localization of GFP-tagged Sqh (Sqh:GFP) in live border cells. Our previous study showed that Sqh:GFP coalesces into discrete, highly dynamic foci at the cluster
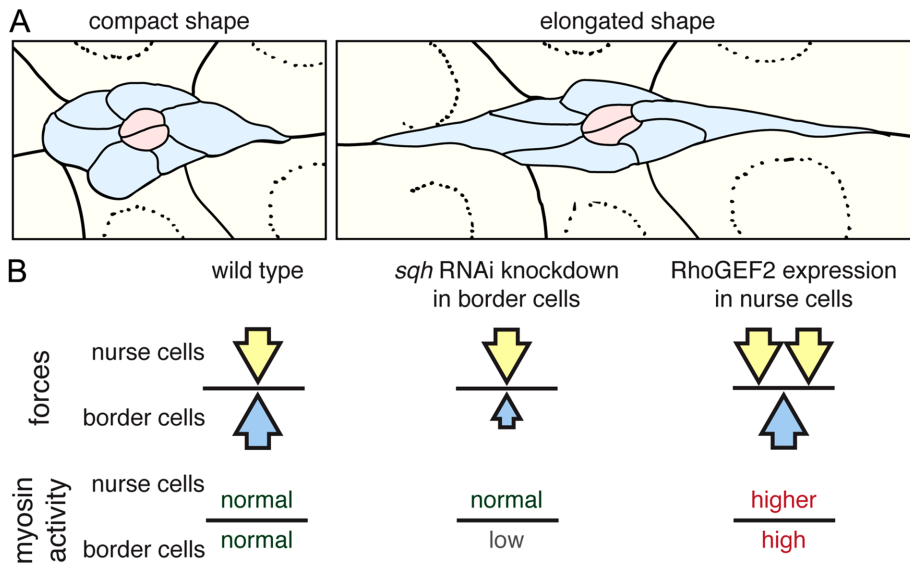
FIGURE 6: Proposed model for maintaining the collective morphology of border cells migrating within the egg chamber. (A) The border cell cluster maintains a collective morphology while migrating between the large nurse cells. (B) A balance of forces (arrows), through actomyosin activity and cortical tension, between nurse cells (yellow) and border cells (blue) produces a compact cluster shape. (A and B) Right, when forces become unbalanced, for example by altered myosin activity, the collective migratory morphology is disrupted. Either knocking down *Sqh* in border cells or expressing ectopic RhoGEF2 in nurse cells causes the border cell cluster to elongate and stop migrating. Border cells respond to increased levels of compressive forces from the surrounding nurse cells by elevating the levels of activated Myo-II.

periphery (Figure 5G) that are lost upon inhibition of Myo-II phosphorylation (Majumder *et al.*, 2012). These foci resemble those observed using 1P-/2P-Sqh antibodies in fixed border cells (Figure 4, A–A″), suggesting that they represent assembly-competent Myo-II that is activated and can bind to F-actin (Vicente-Manzanares *et al.*, 2009). We performed live time-lapse microscopy of Sqh:GFP fluorescence in conjunction with DIC imaging, which allowed us to explicitly image border cell membranes at the outer edge of the cluster where they contact the nurse cells (Figure 5, H and H′; Supplemental Movie S6). Using this method, we analyzed the dynamics of Sqh:GFP foci versus cluster membrane deflections over time (Figure 5I). The appearance of enriched Sqh:GFP signal strongly correlates with cell membranes that pull inward toward the center of the cluster, whereas disappearance of the Sqh:GFP signal correlates with membranes that relax outwardly (Figure 5I). These cycles, or waves, of Sqh:GFP signal are highly dynamic, with relatively short timescales of ~60 s. Interestingly, Myo-II signal and cluster membrane contractility appear to propagate in both the forward and rearward directions (Supplemental Movie S6). Sqh:GFP foci enrichment thus coincides with contractility of border cell membranes at the cluster periphery during migration. Together these results are consistent with dynamic Myo-II activity producing waves of actomyosin contraction that help maintain border cell cluster morphology during migration.

DISCUSSION
Cells move within complex environments in vivo, interacting with other cells and the ECM. This poses a particular challenge for migrating collectives, because they need to withstand extracellular forces without falling apart or becoming greatly disorganized. The mechanisms that govern the impact of tissues on the structural organization of collectives have been unclear because of the difficulty of studying these processes within the native tissue. Here we show

that the border cell collective maintains a specific morphology during its entire migration to the oocyte (Figure 6A). There is very little apparent space separating adjacent nurse cells; nonetheless, border cells efficiently navigate between nurse cells. In contrast to cells that move through the ECM and require proteolytic enzymes to create a pathway (Wolf and Friedl, 2011), the "cell-on-cell" type of migration used by border cells appears to be independent of proteases (Montell *et al.*, 2012). We propose instead that reciprocal mechanical interactions between nurse cells and border cells facilitate the movement of border cells within the cell-dense environment of the egg chamber.

Although nurse cells are known to function as the migratory substrate for border cells, we show that they also impose force upon migrating border cells. The egg chamber is elliptical at this stage and is surrounded by a layer of follicle cells, a basement membrane, and the muscle sheath, which together constrain the overall shape of the tissue (Cetera and Horne-Badovinac, 2015; Andersen and Horne-Badovinac, 2016). We propose that such geometry, in turn, drives an inward, anisotropic force from the nurse cells that imposes tension upon border cells perpendicular to the migration pathway. The border cell cluster actively resists compressive forces from the nurse cells (Figure 6B). The periodic nature of Sqh:GFP indicates that border cells have an intrinsic mechanism to rapidly enrich Myo-II at the cluster periphery during their movement between nurse cells. Specifically, upon nurse cell constriction, local and dynamic activation of Myo-II helps border cells resist this pressure. When forces become imbalanced, either through loss of activated Myo-II in border cells or by elevated cortical tension of nurse cells, the border cell cluster elongates (Figure 6, A and B). Cluster elongation likely occurs along the migration pathway, because the forces imposed by nurse cells are greater in this direction.

Our study also suggests that border cells and their migratory substrate, the nurse cells, each have a certain level of flexibility required for optimal migration. An open question is how nurse cell deformability is regulated at the global level, as well as more locally as border cells move between these large cells. Here we used Rho-GEF2 to ectopically elevate Myo-II activation in all nurse cells through actomyosin-based contraction and tension (Figure 6B; Rogers *et al.*, 2004). Endogenous Myo-II levels are not very high in nurse cells (Edwards and Kiehart, 1996), suggesting that Myo-II is unlikely to be the sole regulator of nurse cell membrane pliability. Further work will be needed to identify the specific combination of factors, such as membrane lipids, associated cortical membrane proteins, and/or cross-linked F-actin (reviewed by Diz-Muñoz *et al.*, 2013; Clark *et al.*, 2014), that influence the malleability of nurse cell membranes.

How does actomyosin-driven tension help border cells maintain a compact morphology? Myo-II accumulates at the periphery of cells undergoing mitosis, increasing intracellular pressure and cortical tension; this in turn allows a cell to resist external deformation (Ramanathan *et al.*, 2015). Similar actomyosin contractility at the

periphery of the border cell cluster thus could increase surface tension to maintain cellular organization. In physics, surface tension is inversely proportional to surface area. Small groups of cells, such as border cells or tumor clusters, often have a small surface area and pronounced curvature (this study; Yamamoto *et al.*, 1983; Friedl *et al.*, 1995; Hidalgo-Carcedo *et al.*, 2011; Montell *et al.*, 2012). However, Myo-II also is able to minimize cell-surface curvature of branching endothelial cells cultured in a three-dimensional microenvironment (Elliott *et al.*, 2015). Our observation that Sqh:GFP and phosphorylated Myo-II each localizes to discontinuous foci on outer cluster membranes may help resolve these two seemingly contradictory ideas. Local enrichment of Myo-II at the cluster periphery, coupled with F-actin, could produce regions of transient lower curvature that help the cluster keep its shape. Indeed, border cells produce periodic dynamic waves of intense Sqh:GFP signal that correlate with local deformation of outer cluster membranes. Similarly, fibroblasts in suspension undergo oscillating cell shape changes that depend on actomyosin contractility through dynamic distribution of F-actin and Myo-II (Paluch *et al.*, 2005; Salbreux *et al.*, 2007). Periodic enrichment of Myo-II at the cluster periphery therefore could promote sufficient cortical tension to rapidly and reversibly adjust the cell cortex in response to changes in the surrounding tissue. We propose that, at the scale of the collective, such local membrane deformations jointly sustain cluster-wide organization and shape.

Our data support a model in which border cell cluster shape requires dynamic regulation of Myo-II activity. Cycles of Sqh/MRLC phosphorylation and dephosphorylation, which correspond to assembly- and disassembly-competent Myo-II, respectively, influence the ability of Myo-II to form bipolar minifilaments and bind to F-actin (Vicente-Manzanares *et al.*, 2009). Phosphomimetic Sqh-EE locks Myo-II into an active conformation but does not rescue the border cell cluster elongation phenotype caused by loss of the activating kinase Rok. Further highlighting the importance of dynamic cycles of Sqh phosphorylation, Myo-II that contains phosphomimetic Sqh fails to undergo contractile pulses, becomes more stabilized, and cannot support morphogenesis of *Drosophila* embryonic tissues (Kasza *et al.*, 2014; Vasquez *et al.*, 2014). In biochemical assays, phosphomimetic Sqh/MRLC mutants do not have as high an activity as endogenously phosphorylated Myo-II (Kamisoyama *et al.*, 1994). Nonetheless, Sqh-EE strongly rescues Rok-dependent defects in border cell detachment and protrusion retraction and mildly suppresses migration defects. The failure of Sqh-EE to rescue the *Rok* RNAi cluster morphology defect therefore suggests that normal cluster shape requires greater cycling of Myo-II activity. At present, however, we cannot rule out a need for higher levels of phosphorylated Sqh. High levels of sustained Myo-II activation, such as through constitutively active RhoA or *Mbs* RNAi, are detrimental to the structure of the cluster because they induce continuous contraction of cells (Majumder *et al.*, 2012; this study).

Myo-II has a surprising number of functions in migrating border cells, with roles in protrusion retraction (Fulga and Rørth 2002), detachment from the anterior epithelium (Edwards and Kiehart 1996; Majumder *et al.*, 2012), and rotation of the cluster (Combedazou *et al.*, 2016). We suggest that, in addition, dynamic Myo-II at the cluster periphery contributes to efficient border cell migration. How can localized dynamic Myo-II promote the movement of collectives? The restriction of activated Myo-II to outer collective surfaces has been proposed to keep cells together so they move as coordinated units with single leader cells (Hidalgo-Carcedo *et al.*, 2011; Reffay *et al.*, 2014). Our data show that dynamic Myo-II promotes the shape of the collective at the supracellular level.

Such a morphology could allow the group to withstand constraints from the surrounding environment to be able to migrate. In this model, dynamic Myo-II creates waves of contraction to help collectives push through the tissue. Cancer cell collectives that migrate in a protease-independent manner do so by pushing through three-dimensional ECM in vitro (Ilina *et al.*, 2011). Moreover, nonadherent migrating cells can use actomyosin cortical flows to propel cells forward in confined environments (Bergert *et al.*, 2015). These studies raise the intriguing possibility that migrating border cells use Myo-II–dependent contraction to squeeze between nurse cells. The phenomenon of balanced opposing forces, coupled to actomyosin contraction, which determines the shapes of collectives that move in tissues, has been difficult to model in vitro. Therefore our results further highlight the importance of studying migrating cells, both single cells and collectives, in their native microenvironment.

MATERIALS AND METHODS
Drosophila strains and genetics
Crosses were performed at 25°C, except *tub*-GAL80^ts ("tsGAL80") crosses, which were set up at 18°C. The following *Drosophila* stocks were obtained from the Bloomington Drosophila Stock Center, Bloomington, IN (unless otherwise indicated), and are described in FlyBase (http://flybase.org): *hsp70*-GAL4 (*hs*-GAL4), *sqh*^AX3 FRT 19A, *Rok*^2 FRT 19A, FRT 19A, *c306*-GAL4, *slbo*-GAL4, *tub*-GAL80^ts ("tsGAL80"), *matalpha4-GAL-VP16*-GAL4 ("nurse cell GAL4"), UAS-mCD8:GFP, UAS-Rho1.V14 ("RhoA^V14"), UAS-Venus:Rok^K116A ("Rok KD"; from J. Zallen, Memorial Sloan Kettering Cancer Center, New York, NY), UASp-T7.RhoGEF2, UAS-*sqh* RNAi (line 7916; Vienna *Drosophila* Resource Center [VDRC]; Vienna, Austria), UAS-*Mbs* RNAi (line 105762; VDRC), UAS-*Rok* RNAi (line 9774R-2; National Institute of Genetics Fly Stock Center [NIG-Fly]; Kyoto, Japan), UAS-*Drak* RNAi (line 107263, VDRC), UAS-GFP dsRNA ("GFP RNAi"), *sqh-sqh*^E20E21:FLAG ("Sqh-EE") and *sqh*^AX3; *sqh*-Sqh:GFP (III) ("Sqh:GFP"; from R. Karess, Paris Diderot University, Paris, France), *sqh-sqh*^A20A21:FLAG ("Sqh-AA"; from L. Luo, Stanford University, Palo Alto, CA), and ubi-Rok:GFP (from V. Mirouse, Clermont Université, Clermont-Ferrand, France). The *w*^1118 line was used as a wild-type control.

Mosaic mutant clones of *sqh*^AX3 FRT 19A, *Rok*^2 FRT 19A, and control FRT 19A were produced by the FLP-FRT system (Xu and Rubin, 1993) using the *ubi-mRFP.nls hsFLP FRT 19A* stock. Homozygous mutant cell clones were marked by loss of nuclear mRFP. Three- to 5-d-old flies of the correct genotype were selected and heat shocked for 1 h at 37°C, twice a day for 2 d; this was followed by recovery at 25°C for 5 d. Clones for *sqh*^AX3, FRT 19A, and FRT 19A control were generated previously (Majumder *et al.*, 2012) but were reanalyzed independently to assess cluster shape (Figure 3, F and G). Few completely mutant *sqh*^AX3 or *Rok*^2 clusters were found.

GAL4 lines were outcrossed to *w*^1118 as controls. *slbo*-GAL4 was used to overexpress proteins uniformly and at high levels in all border cells (Rørth *et al.*, 1998; Laflamme *et al.*, 2012). *c306*-GAL4 was used to express UAS-RNAi lines in anterior follicle cells and border cells. *c306*-GAL4 is expressed earlier in oogenesis than *slbo*-GAL4 and generally achieves more efficient RNAi knockdown (Murphy and Montell, 1996; Aranjuez *et al.*, 2012; Laflamme *et al.*, 2012). To induce optimal GAL4/UAS overexpression and RNAi knockdown, we incubated flies overnight (14–18 h) at 29°C before dissection. *matalpha4-GAL-VP16*-GAL4 ("nurse cell GAL4") was used to overexpress RhoGEF2 in nurse cells (Hudson and Cooley, 2014; Spracklen *et al.*, 2014). Expression of RhoGEF2 using the nurse cell GAL4 was achieved by incubating flies at 27°C. RhoGEF2 expression can cause

nurse cell membrane breakdown in some egg chambers; these egg chambers were identified using phalloidin, which stains F-actin enriched at nurse cell membranes, and were excluded from our analyses.

The tsGAL80 line was used to suppress c306-GAL4/UAS-RNAi during early stages of oogenesis in which an RNAi line could be cell lethal. UAS-sqh RNAi (VDRC 7196) phenotypes were stronger when using c306-GAL4, tsGAL80 compared with c306-GAL4 (Majumder et al., 2012). The enhanced phenotype is presumably due to increased viability of cells with the greatest knockdown, since the pattern of c306-GAL4 expression with or without tsGAL80 was identical in anterior follicle cells and border cells (Supplemental Figure S3). Crosses with tsGAL80 were kept at 18°C to suppress GAL4-UAS (McGuire et al., 2004a,b). Before dissection, flies were heat shocked at 37°C for 1 h, followed by a shift to 29°C for 18–24 h to completely turn off GAL80 and turn on GAL4/UAS.

Immunostaining

Ovaries were dissected and antibody stained as previously described (McDonald and Montell, 2005). Fixation was generally in 4% methanol-free formaldehyde (Polysciences, Warrington, PA) in phosphate buffer (pH 7.4) for 10 min. For 1P-Sqh and 2P-Sqh staining, fixation was in fresh 4% paraformaldehyde (Polysciences) in PBT (1× phosphate-buffered saline, pH 7.2, 0.1% Triton X-100) for 20 min. Primary antibodies from the Developmental Studies Hybridoma Bank (DSHB; University of Iowa, Iowa City, IA) were used at the following dilutions: 1:100 mouse anti-Arm (N27A1); 1:10 rat anti–E-cad (DCAD2); 1:10 mouse anti-GFP (12A6); 1:10 mouse anti-Rho1 (p1D9); 1:50 mouse anti-Fascin (Sn7C). Other antibodies used in this study were: 1:100 mouse anti-FLAG (M2; Sigma-Aldrich, St. Louis, MO), 1:1000 guinea pig anti–1P-Sqh and 1:500 rat anti–2P-Sqh (from R. Ward, University of Kansas, Lawrence, KS). Secondary antibodies conjugated to Alexa Fluor 488, 568, or 647 (Thermo Fisher Scientific, Waltham, MA) were used at 1:400. Alexa Fluor 568–phalloidin (1:400; Thermo Fisher Scientific) was used to label F-actin, and 4′,6-diamidino-2-phenylindole (DAPI; 0.05 μg/ml; Sigma-Aldrich) was used to label nuclei. Egg chambers were mounted in Aqua-Poly/Mount (Polysciences) before being imaged.

Imaging and analyses

Micrographs were acquired using the Zeiss AxioImager Z1 microscope (Carl Zeiss, Thornwood, NY), Zeiss ApoTome system, and an MRm CCD camera with a 20× Plan-Apochromat 0.75 numerical aperture (NA) or a 40× Plan-Neofluar 1.3 NA, oil-immersion objective. The z-stack images acquired from live imaging of Sqh:GFP were processed using the Zeiss Axiovision 4.8 deconvolution software module. Live imaging was performed as previously described (Prasad et al., 2007; Majumder et al., 2012). For visualization of nurse cell membranes (e.g., Figure 1B and Supplemental Movie S1), the lipophilic dye FM 4-64 (Thermo Fisher Scientific) was added at 9 μM final concentration to the culture media during preparation and imaging of live dissected egg chambers (Bianco et al., 2007; Prasad et al., 2007). Kohler illumination was optimized to perform DIC time-lapse live imaging. Movies were created using the Axiovision 4.8 Inside 4D software module or ImageJ. Image brightness and/or contrast of images were adjusted in the ImageJ distribution Fiji (http://fiji.sc; Schindelin et al., 2012), Adobe Photoshop (Adobe, San Jose, CA), or Zeiss Axiovision 4.8 software.

Measurements of nurse cell shape, border cell cluster length, protrusion length, and mean pixel intensity were done using Fiji. Nurse cell shape was measured using the Analyze Particles function of Fiji. Briefly, individual nurse cell regions of interest (ROIs) were obtained by manually filling in the area bounded by the nurse cell membranes and were subjected to the Analyze Particles function. The function provides values for nurse cell ROI area and circularity. A circularity value of 1.0 indicates a perfect circle, while values approaching 0.0 represent extremely elongated shapes. For measuring cluster length, the outlines of clusters and protrusions in midmigration were defined by Fascin immunofluorescence (fixed samples) or mCD8:GFP expression (live samples). The overall length of the cluster was measured along the migration axis but excluded cellular protrusions. Protrusions and the cluster body were defined similar to the criteria of Poukkula et al. (2011). Briefly, the entire cluster, including protrusions, was identified by Fascin staining. The cluster body was defined by the unstained border cell nuclei and surrounding Fascin-positive cytoplasm. The protrusions were defined as cellular "extensions" away from the cluster body that lack nuclei and are narrower than the cluster body (Poukkula et al., 2011). Backward extensions were not included in these analyses. Protrusion length was measured manually and defined as the distance from the tip of the protrusion to its base, where it meets the main cluster body (Majumder et al., 2012).

For measuring mean pixel intensity, control and RhoA^{V14} clusters were stained for 1P-Sqh and 2P-Sqh simultaneously and imaged using the same exposure settings. The cluster was defined by border cell–specific slbo-GAL4 > mCD8:GFP expression. For measuring the mean pixel intensity of 2P-Sqh staining in border cells from nurse cell > RhoGEF2 egg chambers, the border cell cluster was defined by Fascin staining. A new image was created to measure pixel intensity only within the area of the border cell cluster. The pseudocolor heat map images of 2P-Sqh–stained border cell clusters were generated using the Fiji Lookup Table function. The Fiji Reslice function was used to generate kymographs from movies after a common-line ROI was defined in the GFP and DIC channels. RNAi knockdown efficiency was measured from reverse transcription PCR (RT-PCR) products run on gels using the Fiji Gel Analyzer function.

RT-PCR

For measuring RNAi efficiency (Supplemental Figure S2), UAS-RNAi transgenes were expressed in whole flies using hs-GAL4 to achieve ubiquitous knockdown. Flies were subjected to heat shock for 1 h at 37°C twice a day on 2 consecutive days; this was followed by 29°C recovery overnight. Total RNA was isolated from 10 to 15 whole-fly carcasses. Trizol-extracted RNA was used for cDNA synthesis followed by RT-PCR, as previously described (Aranjuez et al., 2012). RT-PCR was performed using the Superscript III One-Step RT-PCR system (Thermo Fisher Scientific). PCR settings were as follows: 50°C for 30 min during the cDNA synthesis step; 55°C for 30 s during the annealing step; 72°C for 1 min during the extension step. The number of PCR cycles was empirically determined for each reaction and primer set to avoid the plateau phase of PCR amplification; 29 cycles were used for both sqh and Rok. Band intensities of the RT-PCR products were measured using ImageJ (Schneider et al., 2012). GAPDH was used as the reference gene. The gene-specific primers used were as follows: sqh fwd, TCACACTTGGCCTTCTC-GTC; sqh rev, CGAGATAGTCGTCCGTTGGG; Rok fwd, AGGAAC-GCGTCTCACTCAAG; Rok rev, GTGAGGGAGAGCAGAGAGGA; GAPDH fwd, ACTCATCAACCCTCCCCCG; GAPDH rev, GCGGAC-GGTAAGATCCACAA.

Figures, graphs, and statistics

Figures and illustrations were created in Adobe Illustrator CS5. GraphPad Prism (GraphPad Software, La Jolla, CA) was used to generate graphs and statistical analyses (unpaired t test and one-way analysis of variance [ANOVA]).

REFERENCES

Alexander S, Weigelin B, Winkler F, Friedl P (2013). Preclinical intravital microscopy of the tumour-stroma interface: invasion, metastasis, and therapy response. Curr Opin Cell Biol 25, 659–671.

Amano M, Ito M, Kimura K, Fukata Y, Chihara K, Nakano T, Matsuura Y, Kaibuchi K (1996). Phosphorylation and activation of myosin by Rho-associated kinase (Rho-kinase). J Biol Chem 271, 20246–20249.

Amano M, Nakayama M, Kaibuchi K (2010). Rho-kinase/ROCK: A key regulator of the cytoskeleton and cell polarity. Cytoskeleton 67, 545–554.

Andersen D, Horne-Badovinac S (2016). Influence of ovarian muscle contraction and oocyte growth on egg chamber elongation in *Drosophila*. Development 143, 1375–1387.

Aranjuez G, Kudlaty E, Longworth MS, McDonald JA (2012). On the role of PDZ domain-encoding genes in *Drosophila* border cell migration. G3 (Bethesda) 2, 1379–1391.

Bardet PL, Guirao B, Paoletti C, Serman F, Léopold V, Bosveld F, Goya Y, Mirouse V, Graner F, Bellaiche Y ((2013). PTEN controls junction lengthening and stability during cell rearrangement in epithelial tissue. Dev Cell 25, 534–546.

Bastock R, Strutt D (2007). The planar polarity pathway promotes coordinated cell migration during *Drosophila* oogenesis. Development 134, 3055–3064.

Beccari S, Teixeira L, Rørth P (2002). The JAK/STAT pathway is required for border cell migration during *Drosophila* oogenesis. Mech Dev 111, 115–123.

Bergert M, Erzberger A, Desai RA, Aspalter IM, Oates AC, Charras G, Salbreux G, Paluch EK (2015). Force transmission during adhesion-independent migration. Nat Cell Biol 17, 524–529.

Bianco A, Poukkula M, Cliffe A, Mathieu J, Luque CM, Fulga TA, Rørth P (2007). Two distinct modes of guidance signalling during collective migration of border cells. Nature 448, 362–365.

Bronsert P, Enderle-Ammour K, Bader M, Timme S, Kuehs M, Csanadi A, Kayser G, Kohler I, Bausch D, Hoeppner J, et al. (2014). Cancer cell invasion and EMT marker expression: a three-dimensional study of the human cancer-host interface. J Pathol 234, 410–422.

Cai D, Chen S-C, Prasad M, He L, Wang X, Choesmel-Cadamuro V, Sawyer JK, Danuser G, Montell DJ (2014). Mechanical feedback through E-cadherin promotes direction sensing during collective cell migration. Cell 157, 1146–1159.

Cant K, Knowles BA, Mooseker MS, Cooley L (1994). *Drosophila* singed, a fascin homolog, is required for actin bundle formation during oogenesis and bristle extension. J Cell Biol 125, 369–380.

Cetera M, Horne-Badovinac S (2015). Round and round gets you somewhere: collective cell migration and planar polarity in elongating *Drosophila* egg chambers. Curr Opin Genet Dev 32, 10–15.

Choi J-C, Jung H-R, Doh J (2013). Dynamic modulation of small-sized multicellular clusters using a cell-friendly photoresist. ACS Appl Mater Interfaces 5, 12757–12763.

Clark AG, Vignjevic DM (2015). Modes of cancer cell invasion and the role of the microenvironment. Curr Opin Cell Biol 36, 13–22.

Clark AG, Wartlick O, Salbreux G, Paluch EK (2014). Stresses at the cell surface during animal cell morphogenesis. Curr Biol 24, R484–R494.

Combedazou A, Choesmel-Cadamuro V, Gay G, Liu J, Dupré L, Ramel D, Wang X (2016). Myosin II governs collective cell migration behaviour downstream of guidance receptor signalling. J Cell Sci, doi: 10.1242/jcs.179952.

Diz-Muñoz A, Fletcher DA, Weiner OD (2013). Use the force: membrane tension as an organizer of cell shape and motility. Trends Cell Biol 23, 47–53.

Doyle AD, Petrie RJ, Kutys ML, Yamada KM (2013). Dimensions in cell migration. Curr Opin Cell Biol 25, 642–649.

Edwards KA, Kiehart DP (1996). *Drosophila* nonmuscle myosin II has multiple essential roles in imaginal disc and egg chamber morphogenesis. Development 122, 1499–1511.

Elliott H, Fischer RS, Myers KA, Desai RA, Gao L, Chen CS, Adelstein RS, Waterman CM, Danuser G (2015). Myosin II controls cellular branching morphogenesis and migration in three dimensions by minimizing cell-surface curvature. Nat Cell Biol 17, 137–147.

Friedl P, Gilmour D (2009). Collective cell migration in morphogenesis, regeneration and cancer. Nat Rev Mol Cell Biol 10, 445–457.

Friedl P, Locker J, Sahai E, Segall JE (2012). Classifying collective cancer cell invasion. Nat Cell Biol 14, 777–783.

Friedl P, Noble PB, Walton PA, Laird DW, Chauvin PJ, Tabah RJ, Black M, Zänker KS (1995). Migration of coordinated cell clusters in mesenchymal and epithelial cancer explants in vitro. Cancer Res 55, 4557–4560.

Friedl P, Wolf K (2010). Plasticity of cell migration: a multiscale tuning model. J Cell Biol 188, 11–19.

Friedl P, Wolf K, Zegers MM (2014). Rho-directed forces in collective migration. Nat Cell Biol 16, 208–210.

Fulga TA, Rørth P (2002). Invasive cell migration is initiated by guided growth of long cellular extensions. Nat Cell Biol 4, 715–719.

Ghiglione C, Devergne O, Georgenthum E, Carballès F, Médioni C, Cérézo D, Noselli S (2002). The *Drosophila* cytokine receptor Domeless controls border cell migration and epithelial polarization during oogenesis. Development 129, 5437–5447.

Grassie ME, Moffat LD, Walsh MP, MacDonald JA (2011). The myosin phosphatase targeting protein (MYPT) family: a regulated mechanism for achieving substrate specificity of the catalytic subunit of protein phosphatase type 1δ. Arch Biochem Biophys 510, 147–159.

Hacker U, Perrimon N (1998). DRhoGEF2 encodes a member of the Dbl family of oncogenes and controls cell shape changes during gastrulation in *Drosophila*. Genes Dev 12, 274–284.

Hidalgo-Carcedo C, Hooper S, Chaudhry SI, Williamson P, Harrington K, Leitinger B, Sahai E (2011). Collective cell migration requires suppression of actomyosin at cell-cell contacts mediated by DDR1 and the cell polarity regulators Par3 and Par6. Nat Cell Biol 13, 49–58.

Hudson AM, Cooley L (2014). Methods for studying oogenesis. Methods 68, 207–217.

Ilina O, Bakker G-J, Vasaturo A, Hofmann RM, Friedl P (2011). Two-photon laser-generated microtracks in 3D collagen lattices: principles of MMP-dependent and -independent collective cancer cell invasion. Phys Biol 8, 015010.

Ishizaki T, Maekawa M, Fujisawa K, Okawa K, Iwamatsu A, Fujita A, Watanabe N, Saito Y, Kakizuka A, Morii N, et al. (1996). The small GTP-binding protein Rho binds to and activates a 160 kDa Ser/Thr protein kinase homologous to myotonic dystrophy kinase. EMBO J 15, 1885–1893.

Jordan P, Karess R (1997). Myosin light chain-activating phosphorylation sites are required for oogenesis in *Drosophila*. J Cell Biol 139, 1805–1819.

Kamisoyama H, Araki Y, Ikebe M (1994). Mutagenesis of the phosphorylation site (serine 19) of smooth muscle myosin regulatory light chain and its effects on the properties of myosin. Biochemistry 33, 840–847.

Kasza KE, Farrell DL, Zallen JA (2014). Spatiotemporal control of epithelial remodeling by regulated myosin phosphorylation. Proc Natl Acad Sci USA 111, 11732–11737.

Kim JH, Ren Y, Ng WP, Li S, Son S, Kee YS, Zhang S, Zhang G, Fletcher DA, Robinson DN, et al. (2015). Mechanical tension drives cell membrane fusion. Dev Cell 32, 561–573.

Kimura K, Ito M, Amano M, Chihara K, Fukata Y, Nakafuku M, Yamamori B, Feng J, Nakano T, Okawa K, et al. (1996). Regulation of myosin phosphatase by Rho and Rho-associated kinase (Rho-kinase). Science 273, 245–248.

Laevsky G, Knecht DA (2003). Cross-linking of actin filaments by myosin II is a major contributor to cortical integrity and cell motility in restrictive environments. J Cell Sci 116, 3761–3770.

Laflamme C, Assaker G, Ramel D, Dorn JF, She D, Maddox PS, Emery G (2012). Evi5 promotes collective cell migration through its Rab-GAP activity. J Cell Biol 198, 57–67.

Leong MC, Vedula SRK, Lim CT, Ladoux B (2013). Geometrical constraints and physical crowding direct collective migration of fibroblasts. Commun Integr Biol 6, e23197.

Llense F, Martín-Blanco E (2008). JNK signaling controls border cell cluster integrity and collective cell migration. Curr Biol 18, 538–544.

Luo T, Mohan K, Srivastava V, Ren Y, Iglesias PA, Robinson DN (2012). Understanding the cooperative interaction between myosin ii and actin

cross-linkers mediated by actin filaments during mechanosensation. Biophys J 102, 238–247.

Majumder P, Aranjuez G, Amick J, McDonald JA (2012). Par-1 controls myosin-II activity through myosin phosphatase to regulate border cell migration. Curr Biol 22, 363–372.

Matsui T, Amano M, Yamamoto T, Chihara K, Nakafuku M, Ito M, Nakano T, Okawa K, Iwamatsu A, Kaibuchi K (1996). Rho-associated kinase, a novel serine/threonine kinase, as a putative target for small GTP binding protein Rho. EMBO J 15, 2208–2216.

McDonald JA, Montell DJ (2005). Analysis of cell migration using *Drosophila* as a model system. Methods Mol Biol 294, 175–202.

McGuire SE, Mao Z, Davis RL (2004a). Spatiotemporal gene expression targeting with the TARGET and gene-switch systems in *Drosophila*. Sci Signal 2004, pl6.

McGuire SE, Roman G, Davis RL (2004b). Gene expression systems in *Drosophila*: a synthesis of time and space. Trends Genet 20, 384–391.

Melani M, Simpson KJ, Brugge JS, Montell D (2008). Regulation of cell adhesion and collective cell migration by hindsight and its human homolog RREB1. Curr Biol 18, 532–537.

Mohan K, Luo T, Robinson DN, Iglesias PA (2015). Cell shape regulation through mechanosensory feedback control. J R Soc Interface 12, 20150512.

Montell DJ, Yoon WH, Starz-Gaiano M (2012). Group choreography: mechanisms orchestrating the collective movement of border cells. Nat Rev Mol Cell Biol 13, 631–645.

Munjal A, Lecuit T (2014). Actomyosin networks and tissue morphogenesis. Development 141, 1789–1793.

Murphy AM, Montell DJ (1996). Cell type-specific roles for Cdc42, Rac, and RhoL in *Drosophila* oogenesis. J Cell Biol 133, 617–630.

Narumiya S, Tanji M, Ishizaki T (2009). Rho signaling, ROCK and mDia1, in transformation, metastasis and invasion. Cancer Metastasis Rev 28, 65–76.

Niewiadomska P, Godt D, Tepass U (1999). DE-cadherin is required for intercellular motility during *Drosophila* oogenesis. J Cell Biol 144, 533–547.

Omelchenko T, Vasiliev JM, Gelfand IM, Feder HH, Bonder EM (2003). Rho-dependent formation of epithelial "leader" cells during wound healing. Proc Natl Acad Sci USA 100, 10788–10793.

Paluch E, Piel M, Prost J, Bornens M, Sykes C (2005). Cortical actomyosin breakage triggers shape oscillations in cells and cell fragments. Biophys J 89, 724–733.

Pinheiro EM, Montell DJ (2004). Requirement for Par-6 and Bazooka in *Drosophila* border cell migration. Development 131, 5243–5251.

Poukkula M, Cliffe A, Changede R, Rørth P (2011). Cell behaviors regulated by guidance cues in collective migration of border cells. J Cell Biol 192, 513–524.

Prasad M, Jang AC-C, Starz-Gaiano M, Melani M, Montell DJ (2007). A protocol for culturing *Drosophila melanogaster* stage 9 egg chambers for live imaging. Nat Protoc 2, 2467–2473.

Ramanathan SP, Helenius J, Stewart MP, Cattin CJ, Hyman AA, Muller DJ (2015). Cdk1-dependent mitotic enrichment of cortical myosin-II promotes cell rounding against confinement. Nat Cell Biol 17, 148-159.

Reffay M, Parrini MC, Cochet-Escartin O, Ladoux B, Buguin A, Coscoy S, Amblard F, Camonis J, Silberzan P (2014). Interplay of RhoA and mechanical forces in collective cell migration driven by leader cells. Nat Cell Biol 16, 217–223.

Ren Y, Effler JC, Norstrom M, Luo T, Firtel RA, Iglesias PA, Rock RS, Robinson DN (2009). Mechanosensing through cooperative interactions between myosin ii and the actin crosslinker cortexillin I. Curr Biol 19, 1421–1428.

Rogers SL, Wiedemann U, Häcker U, Turck C, Vale RD (2004). *Drosophila* RhoGEF2 associates with microtubule plus ends in an EB1-dependent manner. Curr Biol 14, 1827–1833.

Rørth P, Szabo K, Bailey A, Laverty T, Rehm J, Rubin GM, Weigmann K, Milán M, Benes V, Ansorge W, *et al*. (1998). Systematic gain-of-function genetics in *Drosophila*. Development 125, 1049–1057.

Royou A, Sullivan W, Karess R (2002). Cortical recruitment of nonmuscle myosin II in early syncytial *Drosophila* embryos: its role in nuclear axial expansion and its regulation by Cdc2 activity. J Cell Biol 158, 127–137.

Salbreux G, Joanny JF, Prost J, Pullarkat P (2007). Shape oscillations of non-adhering fibroblast cells. Phys Biol 4, 268–284.

Schindelin J, Arganda-Carreras I, Frise E, Kaynig V, Longair M, Pietzsch T, Preibisch S, Rueden C, Saalfeld S, Schmid B, *et al*. (2012). Fiji: an open-source platform for biological-image analysis. Nat Methods 9, 676–682.

Schneider CA, Rasband WS, Eliceiri KW (2012). NIH Image to ImageJ: 25 years of image analysis. Nat Methods 9, 671–675.

Silver DL, Montell DJ (2001). Paracrine signaling through the JAK/STAT pathway activates invasive behavior of ovarian epithelial cells in *Drosophila*. Cell 107, 831–841.

Spracklen AJ, Fagan TN, Lovander KE, Tootle TL (2014). The pros and cons of common actin labeling tools for visualizing actin dynamics during *Drosophila* oogenesis. Dev Biol 393, 209–226.

Spradling AC (1993). Developmental genetics of oogenesis. In: The Development of *Drosophila melanogaster*, ed. M Bate and A Martinez-Arias, Cold Spring Harbor, NY: Cold Spring Harbor Laboratory Press, 1–70.

Stewart MP, Helenius J, Toyoda Y, Ramanathan SP, Muller DJ, Hyman AA (2011). Hydrostatic pressure and the actomyosin cortex drive mitotic cell rounding. Nature 469, 226–230.

Stonko DP, Manning L, Starz-Gaiano M, Peercy BE (2015). A mathematical model of collective cell migration in a three-dimensional, heterogeneous environment. PLoS One 10, e0122799.

Ueda K, Murata-Hori M, Tatsuka M, Hosoya H (2002). Rho-kinase contributes to diphosphorylation of myosin II regulatory light chain in nonmuscle cells. Oncogene 21, 5852–5860.

Vasquez CG, Tworoger M, Martin AC (2014). Dynamic myosin phosphorylation regulates contractile pulses and tissue integrity during epithelial morphogenesis. J Cell Biol 206, 435–450.

Vedula SRK, Leong MC, Lai TL, Hersen P, Kabla AJ, Lim CT, Ladoux B (2012). Emerging modes of collective cell migration induced by geometrical constraints. Proc Natl Acad Sci USA 109, 12974–12979.

Vicente-Manzanares M, Ma X, Adelstein RS, Horwitz AR (2009). Non-muscle myosin II takes centre stage in cell adhesion and migration. Nat Rev Mol Cell Biol 10, 778–790.

Winter CG, Wang B, Ballew A, Royou A, Karess R, Axelrod JD, Luo L (2001). *Drosophila* Rho-associated kinase (Drok) links Frizzled-mediated planar cell polarity signaling to the actin cytoskeleton. Cell 105, 81–91.

Wolf K, Friedl P (2011). Extracellular matrix determinants of proteolytic and non-proteolytic cell migration. Trends Cell Biol 21, 736–744.

Wolf K, te Lindert M, Krause M, Alexander S, Riet te J, Willis AL, Hoffman RM, Figdor CG, Weiss SJ, Friedl P (2013). Physical limits of cell migration: control by ECM space and nuclear deformation and tuning by proteolysis and traction force. J Cell Biol 201, 1069–1084.

Xu T, Rubin GM (1993). Analysis of genetic mosaics in developing and adult *Drosophila* tissues. Development 117, 1223–1237.

Yamamoto E, Kohama G-I, Sunakawa H, Iwai M, Hiratsuka H (1983). Mode of invasion, bleomycin sensitivity, and clinical course in squamous cell carcinoma of the oral cavity. Cancer 51, 2175–2180.

Zhang L, Ward RE (2011). Distinct tissue distributions and subcellular localizations of differently phosphorylated forms of the myosin regulatory light chain in *Drosophila*. Gene Expr Patterns 11, 93–104.